Pulsed Bessel beam-induced microchannels on a diamond surface for versatile microfluidic and sensing applications

OTTAVIA JEDRKIEWICZ,[1,*] SANJEEV KUMAR,[2] BELÉN SOTILLO,[3] MONICA BOLLANI,[4] ANDREA CHIAPPINI,[5] MAURIZIO FERRARI,[5] ROBERTA RAMPONI,[3] PAOLO DI TRAPANI,[2] AND SHANE M. EATON[3]

[1]IFN-CNR and CNISM UdR Como, Via Valleggio 11, I-22100 Como, Italy
[2]Department of Science and High Technology, Università dell'Insubria, Via Valleggio 11, 22100 Como, Italy
[3]IFN-CNR and Department of Physics, Politecnico di Milano, Piazza Leonardo da Vinci 32, Milano 20133, Italy
[4]IFN-CNR, L-NESS, Via Anzani 42, 22100 Como, Italy
[5]IFN-CNR CSMFO Lab., Via alla Cascata 56/C, Povo, Trento, 38123, Italy
*ottavia.jedrkiewicz@ifn.cnr.it

Abstract: We present a laser machining method based on the use of pulsed Bessel beams to create, by single pass transverse writing, three-dimensional trench-like microstructures on a synthetic monocrystalline diamond substrate. By tuning the laser pulse energy and the writing speed, it is possible to control the features of the surface trenches obtained and to optimize the resulting high aspect-ratio and low roughness microstructures. This work confirms the potentialities of quasi-stationary beams in ultra-fast laser inscription technology. In particular the presented results show the possibility to fabricate deep and precise microfluidic channels on biocompatible diamond substrates, offering a great potential for biomedical sensing applications.

References and links

1. A. D. Aharonovich, A. D. Greentree, and S. Prawer, "Diamond Photonics," Nat. Photonics **5**(7), 397–405 (2011).
2. B. Sotillo, V. Bharadwaj, J. P. Hadden, M. Sakakura, A. Chiappini, T. T. Fernandez, S. Longhi, O. Jedrkiewicz, Y. Shimotsuma, L. Criante, R. Osellame, G. Galzerano, M. Ferrari, K. Miura, R. Ramponi, P. E. Barclay, and S. M. Eaton, "Diamond photonics platform enabled by femtosecond laser writing," Sci. Rep. **6**(1), 35566 (2016).
3. A. Courvoisier, M. J. Booth, and P. Salter, "Inscription of 3D waveguides in diamond using an ultrafast laser," Appl. Phys. Lett. **109**(3), 031109 (2016).
4. F. Jelezko and J. Wrachtrup, "Single defect centres in diamond: A review," Phys. Status Solidi **203**(13), 3207–3225 (2006).
5. D. D. Awschalom, R. Epstein, and R. Hanson, "The diamond age of spintronics," Sci. Am. **297**(4), 84–91 (2007).
6. L. Childress, R. Walsworth, and M. Lukin, "Atom-like defects: from quantum computers to biological sensors," Phys. Today **67**(10), 38–43 (2014).
7. J. J. Gracio, Q. H. Fan, and J. C. Madaleno, "Diamond growth by chemical vapour deposition," J. Phys. D Appl. Phys. **43**(37), 374017 (2010).
8. J. A. Carlisle, "Precious biosensors," Nat. Mater. **3**(10), 668–669 (2004).
9. Y. Ralchenko, I. Vlasov, V. Frolov, D. Sovyk, A. Karabutov, K. Gogolinsky, and V. Yunkin, "CVD Diamond Films on Surfaces with Intricate Shape," Nanostructures Thin Films and Nanodispersion Strengthened Coatings **155**, 209–220 (2004).
10. R. Müller, P. Schmid, A. Munding, R. Gronmaier, and E. Kohn, "Elements for surface microfluidics in diamond," Diamond Related Materials **13**(4-8), 780–784 (2004).
11. M. Fijalkowski, A. Karczemska, J. M. Lysko, R. Zybala, M. KozaneckI, P. Filipczak, V. Ralchenko, M. Walock, A. Stanishevsky, and S. Mitura, "Nanostructured Diamond Device for Biomedical Applications," J. Nanosci. Nanotechnol. **15**(2), 1006–1013 (2015).
12. A. Datta, Y.-R. Wu, and Y. L. Wang, "Real-time observation of ripple structure formation on a diamond surface under focused ion-beam bombardment," Phys. Rev. B **63**(12), 125407 (2001).

13. F. Picollo, A. Battiato, L. Boarino, and S. Ditalia Tchernij, "Fabrication of monolithic microfluidic channels in diamond with ion beam lithography," Nucl. Instr. And Methods in Phys. Research B. in press.
14. Y. Ando, Y. Nishibayashi, K. Kobashi, T. Hirao, and K. Oura, "Smooth and high-rate reactive ion etching of Diamond," Diamond Related Materials **11**(3-6), 824–827 (2002).
15. R. Gattass and E. Mazur, "Femtosecond laser micromachining in transparent materials," Nat. Photonics **2**(4), 219–225 (2008).
16. G. D. Valle, R. Osellame, and P. Laporta, "Micromachining of photonics devices by femtosecond laser pulses," J. Opt. A, Pure Appl. Opt. **11**(1), 013001 (2009).
17. A. M. Ozkan, A. P. Malshe, T. A. Railkar, W. D. Brown, M. D. Shirk, and P. A. Molian, "Femtosecond laser-induced periodic structure writing on diamond crystals and microclusters," Appl. Phys. Lett. **75**(23), 3716–3718 (1999).
18. Y. Shimotsuma, P. G. Kazansky, J. Qiu, and K. Hirao, "Self-organized nanogratings in glass irradiated by ultrashort light pulses," Phys. Rev. Lett. **91**(24), 247405 (2003).
19. Q. H. Wu, Y. R. Ma, R. C. Fang, Y. Liao, Q. X. Yu, X. L. Chen, and K. Wang, "Femtosecond laser-induced periodic surface structure on diamond film," Appl. Phys. Lett. **82**(11), 1703–1705 (2003).
20. V. R. Bhardwaj, E. Simova, P. P. Rajeev, C. Hnatovsky, R. S. Taylor, D. M. Rayner, and P. B. Corkum, "Optically produced arrays of planar nanostructures inside fused silica," Phys. Rev. Lett. **96**(5), 057404 (2006).
21. M. Shinoda, R. R. Gattass, and E. Mazur, "Femtosecond laser-induced formation of nanometer-width grooves on synthetic single crystal diamond surfaces," J. Appl. Phys. **105**(5), 053102 (2009).
22. M. K. Kumtumalla, K. Rajamudili, N. R. Desai, and V. V. S. S. Srikanth, "Polarization controlled deep sub-wavelength periodic features written by femtosecond laser on nanodiamond thin film surface," Appl. Phys. Lett. **104**(16), 161607 (2014).
23. S. Su, J. Li, G. C. B. Lee, K. Sugden, D. Webb, and H. Ye, "Femtosecond laser-induced microstructures on Diamond for microfluidic sensing device applications," Appl. Phys. Lett. **102**(23), 231913 (2013).
24. J. Durnin, J. Miceli, Jr., and J. H. Eberly, "Diffraction-free beams," Phys. Rev. Lett. **58**(15), 1499–1501 (1987).
25. M. L. Hupert, J. M. Jackson, H. Wang, M. A. Witek, J. Kamande, M. I. Milowsky, Y. E. Whang, and S. A. Soper, "Arrays of High-Aspect Ratio Microchannels for High-Throughput Isolation of Circulating Tumor Cells (CTCs)," Microsyst. Technol. **20**(10-11), 1815–1825 (2014).
26. M. Duocastella and C. B. Arnold, "Bessel and annular beams for materials processing," Laser Photonics Rev. **6**(5), 607–621 (2012).
27. M. K. Bhuyan, F. Courvoisier, P.-A. Lacourt, M. Jacquot, R. Salut, L. Furfaro, and J. M. Dudley, "High aspect ratio nanochannel machining using single shot femtosecond Bessel beams," Appl. Phys. Lett. **97**(8), 081102 (2010).
28. M. K. Bhuyan, F. Courvoisier, H. S. Phing, O. Jedrkiewicz, S. Recchia, P. Di Trapani, and J. Dudley, "Laser micro-and nanostructuring using femtosecond Bessel beams," Eur. Phys. J. Spec. Top. **199**(1), 101–110 (2011).
29. O. Jedrkiewicz, S. Bonanomi, M. Selva, and P. Di Trapani, "Experimental investigation of high aspect ratio tubular microstructuring of glass by means of picosecond Bessel vortices," Appl. Phys., A Mater. Sci. Process. **120**(1), 385–391 (2015).
30. V. Garzillo, V. Jukna, A. Couairon, R. Grigutis, P. Di Trapani, and O. Jedrkiewicz, "Optimization of laser energy deposition for single-shot high aspect ratio microstructuring of thick BK7 glass," J. Appl. Phys. **120**(1), 013102 (2016).
31. M. K. Bhuyan, O. Jedrkiewicz, V. Sabonis, M. Mikutis, S. Recchia, A. Aprea, M. Bollani, and P. Di Trapani, "High-speed laser assisted cutting of strong transparent materials using picosecond Bessel beams," Appl. Phys., A Mater. Sci. Process. **120**(2), 443–446 (2015).
32. M. A. Porras, A. Parola, D. Faccio, A. Dubietis, and P. Di Trapani, "Nonlinear unbalanced Bessel beams: Stationary conical waves supported by nonlinear losses," Phys. Rev. Lett. **93**(15), 153902 (2004).
33. M. K. Bhuyan, F. Courvoisier, P.-A. Lacourt, M. Jacquot, L. Furfaro, M. J. Withford, and J. M. Dudley, "High aspect ratio taper-free microchannel fabrication using femtosecond Bessel beams," Opt. Express **18**(2), 566–574 (2010).
34. Y. Matzuoka, Y. Kizuka, and T. Inoue, "The characteristics of laser micro drilling using Bessel beam," Appl. Phys., A Mater. Sci. Process. **84**(4), 423–430 (2006).
35. H. O. Jeschke and M. E. Garcia, "Theoretical description of the ultra-fast ablation and graphite: dependence of thresholds on pulse duration," Appl. Surf. Sci. **197–198**, 107–113 (2002).
36. W. Yang, O. Auciello, J. E. Butler, W. Cai, J. A. Carlisle, J. E. Gerbi, D. M. Gruen, T. Knickerbocker, T. L. Lasseter, J. N. Russell, Jr., L. M. Smith, and R. J. Hamers, "DNA-modified nanocrystalline diamond thin-films as stable, biologically active substrates," Nat. Mater. **1**(4), 253–257 (2002).
37. A. Härtl, E. Schmich, J. A. Garrido, J. Hernando, S. C. R. Catharino, S. Walter, P. Feulner, A. Kromka, D. Steinmüller, and M. Stutzmann, "Protein-modified nanocrystalline diamond thin films for biosensor applications," Nat. Mater. **3**(10), 736–742 (2004).
38. C. A. Barrios, "Optical Slot-Waveguide Based Biochemical Sensors," Sensors (Basel) **9**(6), 4751–4765 (2009).
39. V. V. Kononenko, V. M. Gololobov, and V. I. Konov, "Laser-induced graphitization of diamond," Appl. Phys., A Mater. Sci. Process. **122**(3), 258–263 (2016).
40. A. C. Ferrari and J. Robertson, "Interpretation of Raman spectra of disordered and amorphous carbon," Phys. Rev. B **61**(20), 14095–14107 (2000).

41. E. Alhadeff and N. Bojorge, *Graphite-Composites Alternatives for Electrochemical Biosensor, Metal, Ceramic and Polymeric Composites for Various Uses*, Dr. John Cuppoletti, ed. IS, InTech (2000), Available from: http://www.intechopen.com/books/metal-ceramic-and-polymericcompositesfor-various-uses/graphite-composites-alternatives-forelectrochemical-biosensor.

1. Introduction

Diamond substrates and films have been adapted for many uses because of the material's exceptional properties such as the highest thermal conductivity, high mechanical hardness, wide bandgap, very good optical properties as well as chemical resistance. Indeed diamond has now rapidly been gaining interest for different applications, such as photonics [1] including optical waveguiding [2,3], and quantum information technologies [4,5] thanks to the properties of the nitrogen-vacancy center [6]. Moreover the advantages of diamond in the field of biosensors are enormous, thanks to its chemical stability, its largest electrochemical potential window, and its biocompatibility, which makes this material preferable with respect to other biocompatible materials [7,8].

However because of its hardness, efficient fabrication methods for diamond are still limited, especially for cases where sub-micron or micron size surface microstructures are needed such as for biosensing or microfluidics applications. Channels in fluidic systems have always been difficult to fabricate, especially in the case of diamond where mold techniques [9–11] with the use of sacrificial layers are usually adopted. Focusing ion beam technology [12,13], or alternatively reactive ion etching [14] have also been used for monolithic microfluidic channels fabrication or surface modification on diamond, with lengthy processes or inefficient etching rates.

In the last few years, the femtosecond (fs) laser technology has seen a considerable growth in scientific and manufacturing communities for its precision and damage free capability [15], enabling the micromachining of different materials for photonics applications [16]. In the case of surface machining of diamond the use of the laser microfabrication technology has been mainly limited to the investigation of the periodical sub-micron ripples observed on the sample surface after laser irradiation [17–22], and to the generation of channel-like structures with an average depth of less than half micron [23].

We propose a novel approach to surface deep microchannel fabrication, exploiting the use of non-diffractive Bessel beams [24]. Indeed the standard laser micromachining techniques making use of focused Gaussian beams, determine a high degree spatial energy confinement with an aspect-ratio given by the focal volume, imposing a constraint on the speed and quality of the microfabrication in some applications where larger dimensions of the machined structures are required. For instance in microfluidics, extended channel depth allows for increased throughput at the optimized flow velocity [25]. Nonconventional beam shapes are more and more under investigation and are designed to meet the requirements of a given material configuration or application that could not be feasible with Gaussian beams [26]. Recently high aspect-ratio microstructuring was demonstrated by focusing a femtosecond pulse in Corning glass (BK7) with a conical lens, in different illumination regimes [27–30], opening the way to high speed deep-drilling and cutting of glass samples [31]. All these results are based on the fact that a Bessel beam is featured by a central core surrounded by rings which constitute the beam energy reservoir for a non-diffracting propagation. In the stationary nonlinear regime [32], a finite energy Bessel beam leaves in its wake a uniform elongated plasma track, generated by the main Bessel lobe, that is the main support for the nonlinear absorption of laser energy. In the present paper we shall use the Bessel beam in transverse writing configuration in such a way to generate an ablation pattern on the diamond substrate surface, featured by micron-sized high aspect-ratio trenches opportunely tailored as a function of the beam parameters and writing speed.

2. The experiment

The laser source used for this experiment is a regeneratively amplified mode-locked Ti:Sapphire laser system delivering 800 nm, 200 fs laser pulses at 20 Hz repetition rate. The Gaussian laser beam, spatially filtered and demagnified is reshaped into a Bessel beam (BB) after being reflected on a spatial light modulator (SLM, Holoeye) imprinting on the beam the phase mask of a conical lens (axicon). The pulse energy is adjusted by means of a half-wave plate combined with a linear polarizer, and measured at the sample position before the micromachining process. Note that the damage energy threshold of our SLM in the fs pulsed regime is about 3 mJ (well above the energy values used in this microfabrication experiment). By changing the axicon angle parameter (linked to the Bessel cone angle θ) we can adjust the Bessel non-diffracting length (Bessel zone) $z_{max} \approx w_0 / \tan\theta$ and the Bessel core radius size $r_0 = 2.4040\lambda / 2\pi\sin\theta$, w_0 being the transverse size of the input beam on the SLM evaluated as full width at half maximum (FWHM) from the intensity transverse profile. The resulting BB, demagnified by a suitable telescopic system constituted by a f = 300 mm lens (L1) and a 0.45 N.A. 20× optical microscope objective (OM1), is injected orthogonally to the surface of a polished synthetic monocrystalline diamond sample (type II, $5 \times 5 \times 0.5$ mm^3, MB Optics), previously mounted and aligned on a computer controlled three-axes motorized translation stage (Aerotech). A scheme of the microfabrication part of the set-up is illustrated in Fig. 1. Before laser writing, the evolution of the intensity beam profile along z is monitored by means of a temporary imaging system (not shown in Fig. 1) in order to quantitatively characterize the length of the Bessel zone. In our case the micromachining is performed with a Bessel beam featured in air by a 20° cone angle, a 0.7 μm central core (FWHM), and a total non-diffracting zone length of about 150 μm. Note that because of the Gaussian shape of the input beam impinging on the SLM phase mask, the intensity profile of the resulting BB is not flat along the propagation direction z, and therefore the relative shift along z between the Bessel zone of the beam and the sample is important for the optimization of the ablation depth of the surface. During the laser writing, a real time imaging onto a CCD camera of the (back-illuminated) sample is realized by means of a telescopic system constituted by the microscope objective OM1 and a 150 mm lens (L2).
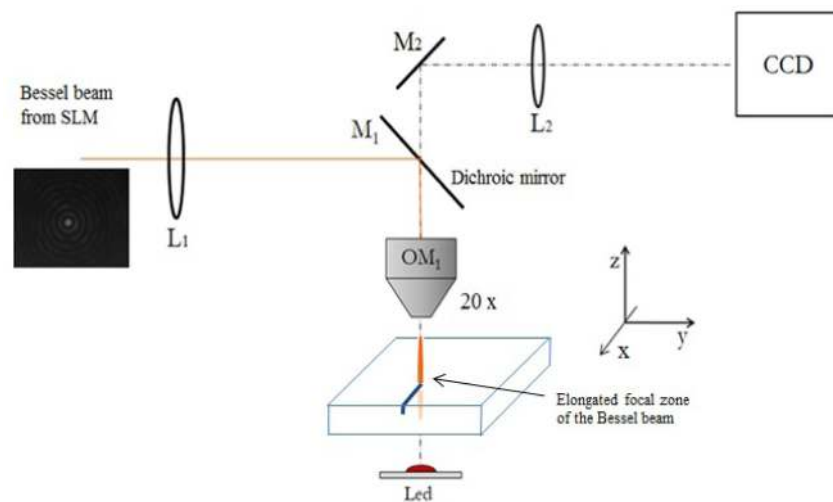

Fig. 1. Scheme of the microfabrication part of the experimental set-up.

3. Results and discussion

We present in Fig. 2 scanning electron microscopy (SEM) images of about 80 μm long tracks written on the diamond surface in different conditions. The top images Fig. 2(a), 2(b) and 2(c) corresponding to trenches both obtained for 100 nm/s writing speed (the low value simply due to the low repetition rate laser available), allow us to appreciate the effect of the pulse total energy on the surface features of the resulting trenches. Note that the time employed to machine tracks as those presented here is of course scalable and can be drastically reduced provided we use a kHz laser, for which thermal effects during the laser fabrication are still negligible, and each laser pulse acts on the material independently. The bottom images Fig. 2(d), 2(e) and 2(f) correspond to tracks obtained for 1 μm/s, 5 μm/s and 10 μm/s respectively (maintaining a fixed energy level). Clearly with a higher laser writing speed the number of pulses spatially superimposed during translation decreases, and consequently lower net fluence results in shallower depths of the central part of the written tracks. In the limit case of single shot (or double shot as in Fig. 2(f)) the track loses its continuity, and separated ablation areas appear. The aspect-ratio of these microstructures, which can be defined as AR = h/d where h is the ablation depth and d is the trench width (at its half depth), reaches AR ≅ 8 for the cases of Fig. 2(a) and Fig. 2(b). It is worth noting that for a given fluence distributed in the focal volume, the ablation process by means of the Bessel beam turns out to be much more efficient with respect to the use of Gaussian beams, for which the Rayleigh range is at least one order of magnitude lower than the Bessel non-diffracting zone. In other words, in order to obtain channels with similar depth, a much smaller number of shots per position (and thus less time) is needed when using Bessel beams.
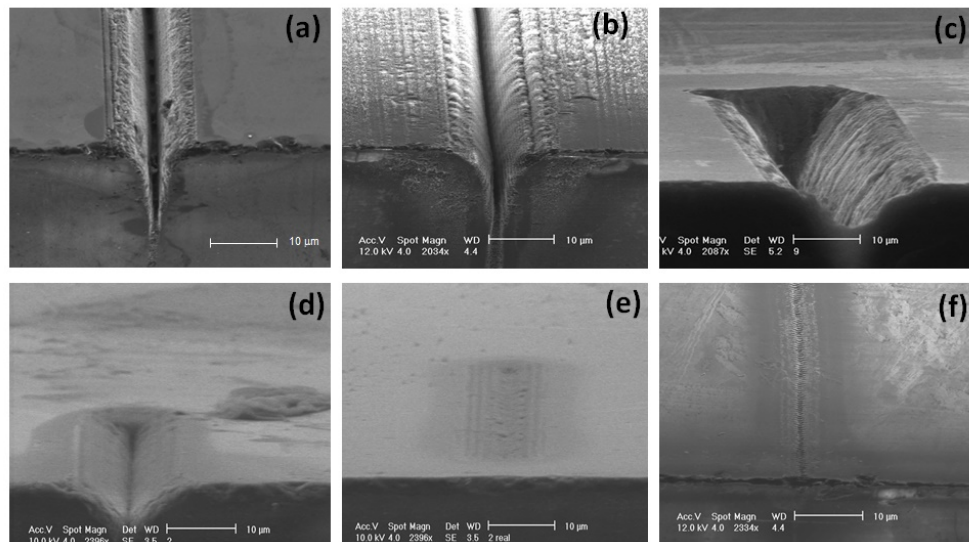

Fig. 2. Tilted view SEM images of microtracks machined in single pass on the diamond surface by means of a femtosecond pulsed Bessel beam with core size of about 0.7 μm (FHWM) in air, for different transverse writing speeds and pulse energies. The scale bar for all SEM images is 10 μm. In (a), (b) and (c) the writing speed corresponded to having 280 spatially superimposed pulses. The energy per pulse was E = 3.5 μJ in (a), 7 μJ in (b) and 10 μJ in (c). The tracks in (d), (e) and (f) have been written with E = 7 μJ and with machining speed such to have respectively 28 (d), 9 (e) and 2 (f) spatially superimposed pulses during the sample translation.

The pulse energy can be adjusted in such a way to exploit only the central lobe of the BB in the radiation-matter interaction for the ablation process (i.e. BB peak intensity greater than

the ablation threshold of the material). Since the peak intensity of the central lobe of the BB is much higher than that of the lateral rings, one can work in a regime where only the BB core is nonlinearly absorbed by the material, with an efficient energy transfer in depth along the propagation into the sample lattice. In the present work, for the energy values used and because of the spatial superposition of the pulses, the lateral rings of the BB affect in any case the side of the written tracks. In particular the traces left by these rings can be clearly seen around most of the V-shaped 3D microstructures of Fig. 2 (in particular in Fig. 2(b)). In general these tracks are featured by a deeper central trench "digged" by the BB central core during the nonlinear absorption process. Note that for the large trench shown in Fig. 2(c) (in this case 10 μm wide), a strong nonlinear absorption of the whole beam has occurred, resulting in an extended and heavy ablation of the material where the imprinting of the Bessel beam intensity profile is no longer observed. It also turns out that for a given beam intensity at the material surface, the angle of the V-shape of the microstructures is directly related to the Bessel beam cone angle. This is in analogy with previous observations related to the effect of the numerical aperture micromachining experiments performed in glass or steel with Bessel beams [33,34]. On the other hand, in the cases presented in this work where the Bessel beam geometry is fixed, while the depth of the trenches is determined by the writing speed, their transverse width depends on the pulse energy. Finally note that considering the equal distribution of the total pulse energy through the rings of the beam, we calculated the fluences associated with the BB core and used here for the surface ablation to be of the order of a few J/cm^2 (from 2 to 6 J/cm^2) thus above the diamond damage threshold [35].

The results presented in Fig. 2 have shown the possibility to tailor the cross-section of the trenches that can be generated (with arbitrary length) at the diamond surface, and potentially useful for ad hoc microfluidics applications, biosensing or analytical tasks, depending for instance on the size of the cells and biomolecules to be detected.

We focus now our attention on the surface pattern ablation of Fig. 2(a). A top view magnified SEM image of a portion of that trench is reported in Fig. 3, showing the presence of a central track surrounded by nanopatterned walls.
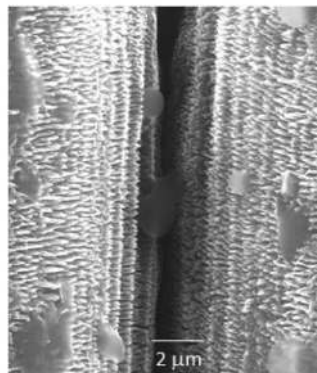

Fig. 3. Top view SEM images of a portion of the trench reported in Fig. 2(a).

A wet etching has been carried out to clean the samples and remove the possible graphitic contamination derived by the laser micromachining process. The chemical wet etching was performed with a solution of H_2SO_4 (96%vol): HNO_3(69%vol): H_2O (with volume ratio 8:4:1) at 70° for 8 h, which as it will be shown later, attacks an eventual graphitic layer but not the diamond substrate [22]. The apparent smoothness and regularity of the high aspect-ratio, 12 μm-depth, ablated structure of Fig. 2(a) is confirmed by the SEM image taken after the etching and shown in Fig. 4(a). Indeed the image reveals the presence of an homogeneous microchannel of about 1.5 μm width, at the very center in depth of the 3D V-shaped trench also featured by nanogrooves at the bottom and on its walls. While in Fig. 4(a) the Bessel

beam polarization was parallel to the sample translation direction, in Fig. 4(b) we present the SEM image of a trench generated with the same laser parameters and writing speed as in Fig. 4(a), but with the sample translation direction orthogonal to the beam polarization. In this case a high aspect-ratio trench similar than before can be fabricated, and its nanogroove fine structure lies now parallel to the microchannel direction.
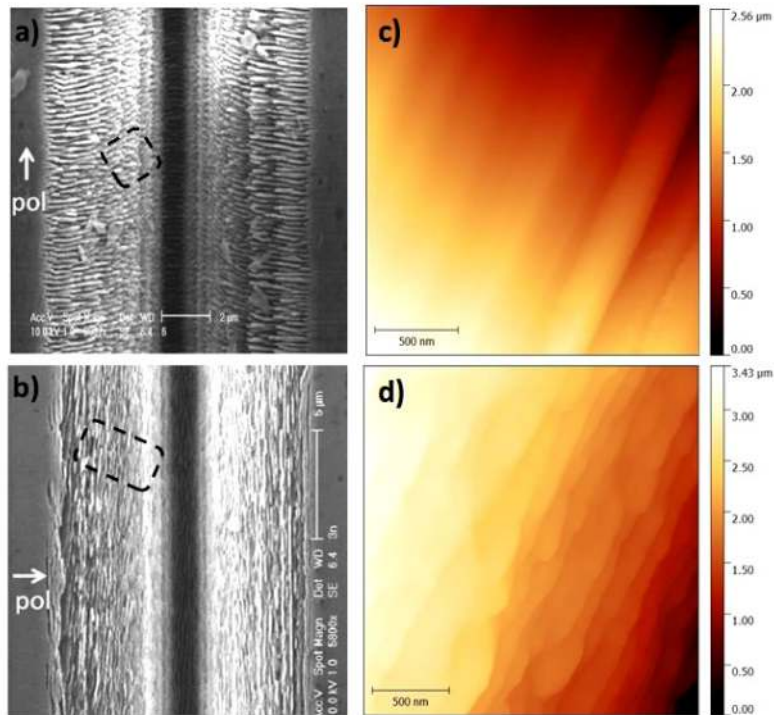

Fig. 4. Top view SEM images of the microchannels formed inside the machined trenches in the conditions of Fig. 2(a), for two different transverse writing directions; respectively parallel (a) and orthogonal (b) to the laser beam polarization. In c) and d) AFM tapping-amplitude images of the labelled (dashed) regions in the SEM images.

The periodic nanostructures observed within the whole ablated region with a periodicity of the order of $\lambda / 2n$ (where n is the material refractive index, and λ the laser wavelength), are in accordance with previous works and are attributed to the interaction between the laser pulse and a laser-induced plasma [19,21]. Note that as expected the nanogrooves lie orthogonally to the laser polarization.

To evaluate the surface roughness of the trench, topography images have been acquired by an atomic force microscope (AFM) in tapping mode with a Veeco Innova instrument, and super-sharp silicon probes (typical radius of curvature 2 nm) have been used for high-resolution imaging of the nanogrooves. AFM images relative to the labelled (dashed) regions of the SEM images of Fig. 4(a) and 4(b) are presented in Fig. 4(c) and 4(d) respectively. The observation of our sample through AFM diagnostics has highlighted an average depth of the nanogrooves lying in the range of 130-150 nm, the estimation having been made by taking 9 linescans in different positions on the AFM topographic images analyzed without any smoothing.

The diamond surface can be relatively easily and reliably functionalized with organic molecules, DNA or enzymes and it is suitable for the attachment of circulating tumor cells (CTC) [36,37]. The possibility to write in a controlled way nanometer-sized substructures inside the trenches of a microfluidic chip can be therefore an added value especially for

biosensing applications, in all cases where the cells to be isolated, based on their biomechanical properties, present a different adhesion to particular nanorough surfaces, or nanogrooves orientation. Finally note that the microchannel roughness (at the subwavelength-scale) may also imply that the generated microchannels might behave as optical slot waveguides, now an emerging field towards the realization of highly sensitive biochemical optical integrated sensors [38].

The diamond substrate was also characterized by micro-Raman spectroscopy in order to show the formation of graphitic-like phase on the tracks after the laser irradiation [39]. Micro-Raman spectra were recorded by means of a Labram Aramis John Yvon Horiba system with a DPSS laser source at 532 nm and equipped with a confocal microscope and an air-cooled CCD. A 100× objective was used to focus the laser on the sample as well as to collect the Raman signal, with a spatial resolution of about 1 μm. We can achieve a wavenumber accuracy of about 1 cm^{-1} with a 1800 line/mm grating. We report in Fig. 5 the results relative to a trench written in conditions similar to those of Fig. 2(c), that is, in conditions of strong laser irradiation (due to low writing speed and high energy). The spectra measured after the laser irradiation (Fig. 5(b) and 5(c)) on this track featured two peaks: the G-peak centered at 1598 cm^{-1} and the D-peak around 1351 cm^{-1}. These peaks appear in the Raman spectra of various nanocrystalline and amorphous carbons, with position, width and relative intensity depending on the carbon phase [37]. In our case, from their position, relative intensity (I(D)/I(G) ≈1.1) and FHMW of the G-peak (around 70 cm^{-1}) we conclude that nanocrystalline graphite is formed. This behavior follows the trend observed in [2], where lower repetition rates of the femtosecond laser induce the formation of more nanocrystalline graphite clusters. The appearance of second-order Raman peaks (at 2700 cm^{-1} (2D peak) and 2900 cm^{-1} (D + G peak)) is also indicative of ordering of the graphitic-like phase [40]. It is important to note that the diamond crystal peak at 1331 cm^{-1} is not visible in these spectra, because absorption of the graphitic layer does not allow to detect the diamond below.
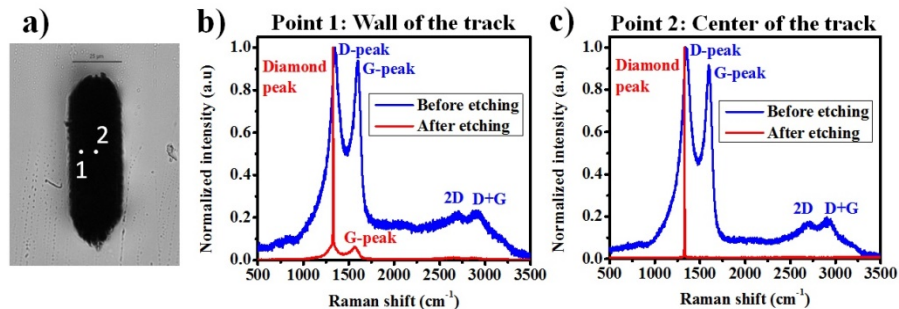

Fig. 5. a) Optical transmission microscope image of a deep trench written by Bessel beam fs laser machining ; b) and c) normalized Raman spectra measured before (blue) and after (red) etching, on a point respectively at the wall and at the bottom center of the machined trench.

The Raman measurements were repeated after the chemical wet etching described before. The graphitic-like layer turns out to be almost completely removed after the chemical etching, as shown in Fig. 5, according to the appearance of the crystal diamond peak coming from the diamond surface of the channel. The detection of weak D and G components on the wall of the trench (Fig. 5(b)) may be attributed to the different wettability of the wall due to its higher roughness, and thus to a less efficient etching process. On the other hand at the bottom of the machined channel, where in addition the etching solution may be driven by the V-shape of the trench, only the diamond peak is detected.

Note that microchannels covered with a graphitic layer may also constitute an advantage in those biosensing application cases where the main purpose of the conducting phase is to supply electrical conductivity needed for the conduction of electrical biosignals [41].

4. Conclusions

To conclude we have shown the possibility to create high aspect-ratio microstructures on monocrystalline diamond by laser transverse writing using femtosecond quasi-stationary micron-sized Bessel beams. These beams thanks to their conical energy reservoir can propagate in depth in the material along distances much higher than the typical Rayleigh range of focused Gaussian beams of equivalent dimensions, allowing thus to obtain ablated trenches with features that depend on the beam parameters and writing speed. This work opens the way to the fabrication of ad hoc smooth and deep microfluidic channels on biocompatible diamond substrates, thus offering a great potential for biomedical sensing applications.